Turkish Journal of Chemistry

http://journals.tubitak.gov.tr/chem/

Research Article

Turk J Chem
(2022) 46: 1607-1619

doi:10.55730/1300-0527.3464

A study of silicon and germanium-based molecules in terms of solar cell devices performance

Emine TANIŞ*

Department of Electrical Electronics Engineering, Faculty of Engineering and Architecture Kırşehir Ahi Evran University, Kırşehir, Turkey

Received: 23.02.2022 • **Accepted/Published Online:** 13.06.2022 • **Final Version:** 05.10.2022

Abstract: Photovoltaic energy sources are increasingly in demand due to the cost of petroleum fuels and concerns about carbon emissions. For this reason, it is important to determine the photovoltaic properties of the compounds that are thought to be suitable for these energy sources. Here, 1,1,2,3,4,5-Hexaphenyl-1H-silole (HPS) and 1,1,2,3,4,5-Hexaphenyl-1H-germole (HPG) compounds that are thought to have excellent photovoltaic properties, electronic and charge transport properties were investigated experimentally and theoretically. The total energies, absorption spectra, Fermi energy (E_{fl}) and work function (ϕ), maximum open circuit voltage (V_{OC}), reorganization energies (λ_e and λ_h), frontier molecular orbital (HOMO and LUMO), the ionization potentials (IPs) and electron affinities (EAs), effective transfer integrals (V_e and V_h), charge transfer rates (W_e and W_h), molecular electrostatic potential (MEP) surface analysis and Natural Bond Orbital (NBO) analysis were determined and the suitability of the results for photovoltaic solar cell devices was interpreted in detail. The absorbance spectra of the HPS and HPG were experimentally examined and compared to the theoretical results. It can be concluded that HPS and HPG would contribute to the application areas of more effective solar cells with determined properties.

Key words: Reorganization energy, charge transfer rate, silole, germole, DFT, solar cell devices

1. Introduction

Solar cells have become a very popular energy source in recent years due to the increasing energy demand. This energy source, obtained via photovoltaic technology, is the form of solar energy converted into electrical energy. It is considered that low-cost and nature-friendly solar energy has great potential to contribute to the solution of energy demand [1,2]. High-performance photovoltaic solar cells are the only way to obtain solar energy with the maximum performance [3,4]. Therefore, it is crucial to pay attention to the materials that will improve the performance of solar cells. π-conjugated organic molecules have common usage areas such as organic photovoltaic (OPV) devices, organic field effect transistors (OFETs) [5–7], due to their favorable molecular orbital energies and donor-acceptor structures. In this context, HPS and HPG molecules based on silicon and germanium are examples of π-conjugated organic compounds.

In the literature, there are studies on the reaction chemistry of many molecules containing silicon and germanium [8–12]. Organic/inorganic silicon-based solar cells are candidate materials utilized to improve the performance of heterojunction devices that are employed to increase the energy produced by different electrical devices such as solar cells and lasers [13,14]. Despite its many disadvantages, silicon solar cells are the most widely used photovoltaic technology in space and terrestrial fields [1]. Similarly, some germanium-based compounds are suitable molecules for photovoltaic devices and plastic electronics due to their photophysical properties [15–19]. Faustov et al. [20] reported that the stability and electron paramagnetic resonance (EPR) parameters depended on the conformation of phenyl groups in cyclopentadiene, silole, germole, 1,2,3,4-Tetraphenylcyclopenta-1,3-diene, 2,3,4,5-tetraphenylsubstituted structures, and their radical anions by using ab anitio and DFT methods. Zhan and coworkers [21] evaluated the electron affinities of 1,1-Diaryl-2,3,4,5-tetraphenylsiloles molecules, which are silole-derived molecules, with experimental and theoretical methods. Zhang et al. [22] determined the aggregation emission behaviors using the photophysical properties of HPS by quantum mechanical and molecular mechanical methods. Weijie and colleagues [23] suggested that the HPS nanobeads synthesized hold promise for future biological applications with their excellent emission stability. Ito et al. [24] investigated

* Correspondence: eminetanis@ahievran.edu.tr

the phase transformation during evaporative crystallization of HPS with different fluorescent colors using aggregation-induced emission (AIE). Tang et al. [25] synthesized a series of molecules including HPS and its derivatives and determined their photoluminescence properties. However, according to our knowledge, there is no study in which the photovoltaic parameters of HPS and HGS materials that affect the performance of photovoltaic solar cells are calculated in detail in the literature. In addition, there is not yet any study on HPG molecule.

The density functional theory (DFT) and time-dependent (TD)-DFT calculations have been extensively used to investigate the electronic and photovoltaic properties of materials [26,27]. Such theoretical studies are important to save time and money and optimize their experimental procedures. The optimization process starts with the determination of the most suitable geometry where the molecule does not have a negative vibration frequency and continues until the comparison with the experimental results. Similarly, reliable results have been obtained using the DFT and Amsterdam density functional (ADF) methods while assessing the suitability of various structures in terms of solar cells and optoelectronics [28–31]. These studies have also revealed the electronic, optical, and charge transfer properties of molecules in detail.

In the current study, photovoltaic and charge transfer parameters were calculated by DFT and ADF methods to determine the performance of HPS and HPG molecules in terms of photovoltaic solar cells. Considering that the relationship between charge transfer processes and absorbance spectrum may be important in structures with π-conjugated systems such as HPS and HPG, experimental absorbance spectrum results were obtained and compared with theoretical results. In addition, MEP and NBO analyses were performed to determine the reactive sites and charge transfer properties of HPS and HGS molecules. With the results obtained, the suitability of the molecules for solar cells was evaluated in detail.

2. Methods

All calculations of the studied molecules were performed using the Gaussian 09 [32] and Amsterdam density functional (ADF2019) [33] programs. Electronic and photovoltaic calculations of HPS and HPG molecules were performed using the TD-DFT/B3LYP/6-311++G(d,p) level of theory.

ADF is a successful computational chemistry software for calculating molecules in terms of structure, electronics, optics, and more [34–36]. Firstly, the dimer structures of HPS and HPG were optimized in the ADF program, and then, the charge transfer properties were calculated.

Charge transfer rates (W) of HPS and HPG are found by the following equation [37–40], known as the Marcus-Hush equation.

$$W = \frac{V^2}{\hbar}\left(\frac{\pi}{\lambda k_B T}\right)^{1/2} \exp\left(-\frac{\lambda}{4k_B T}\right) \tag{1}$$

where λ is the reorganization energy, T is the temperature, V is the effective charge transfer integral, and ħ and k_B are the Planck and Boltzmann constants, respectively.

V_{ij} representing the electronic coupling between intermolecular; depending on the spatial overlap (S_{ij}), charge transfer integrals (J_{ij}), and site energies ($e_{i(j)}$), respectively,

$$V(ij) = \frac{J_{ij} - S_{ij}(e_i + e_j)/2}{1 - S_{ij}^2} \tag{2}$$

The reorganization energy related to the charge transport process in organic solids can be defined in two ways which are the normal mode analysis method and the four-point approximation. The normal mode analysis method divides the total relaxation energy by the contributions from each vibration mode. In the four-point approximation, λ can be represented as in equation 3. The total reorganization energy is the sum of the internal reorganization energies arising from intermolecular vibration and external reorganization energies created by the polarization of the surrounding environment. The external reorganization energy of a few tenths of an electron volt is a very small value [41,42]. Therefore, the internal reorganization energies created by an electron, or a hole have been taken into account in the current paper. Electron (or hole) reorganization energies, λ_e (or λ_h) can be written as follows:

$$\begin{aligned}\lambda_h &= \lambda_1 + \lambda_2 = [E^+(g^0) - E^+(g^+)] + [E^0(g^+) - E^0(g^0)] \\ &= [(E^+(g^0) - E^0(g^0)] - [(E^+(g^+) - E^0(g^+))]\end{aligned} \tag{3}$$

and

$$\lambda_e = \lambda_3 + \lambda_4$$
$$= [E^0(g^-) - E^0(g^0)] + [E^-(g^0) - E^-(g^-)]$$
$$=[E^0(g^-) - E^-(g^-)] - [E^0(g^0) - E^-(g^0)] \quad (4)$$

Here, $E^0(g^0)$ is the energy of the neutral calculated with the optimized structure of the neutral molecule. $E^{+/-}(g^{+/-})$ ($E^+/-(g^0)$) is the energy of cation/anion calculated with the optimized structure of the cation/anion (neutral) geometry. $E^0(g^{+/-})$ is the energy of the neutral molecule calculated with the optimized structure of the cation/anion geometry.

The injection processes of holes and electrons, which affect the performance of the devices, are highly dependent on their stability and energy barriers [43]. There are many studies in the literature about the injection ability of molecules depending on ionization potentials (IPa/IPv), HOMOs, LUMOs, and electron affinities (EA_a/Ea_v) [44–47]. The IP_v/IP_a, Ea_v/EA_a of the studied structures were obtained as follows:

$$IP(v) = E^+(g^0) - E^0(g^0) \quad (5)$$

$$IP(a) = E^+(g^+) - E^0(g^0) \quad (6)$$

$$EA(v) = E^0(g^0) - E^-(g^0) \quad (7)$$

$$EA(a) = E^0(g^0) - E^-(g^-) \quad (8)$$

The open-circuit voltage (V_{OC}) is defined as the voltage in the zero current state and is closely related to charge recombination [48]. The open-circuit voltage (V_{OC}) of photovoltaic molecules can be calculated by [49]:

$$V_{OC} = |E_{HOMO}(Donor)| - |E_{LUMO}(Acceptor)| - 0.3 \quad (9)$$

Here, both HPS and HGS molecules were used as a donor, and a fullerene-derived molecule, $PC_{60}BM$, was used as an acceptor. $PC_{60}BM$ is a molecule with an efficiency higher than 11% in conventional organic solar cells, and it is widely used in calculations [49–51].

Calculation of fermi energy level (E_{fl}) and work function (ϕ) is important for photoelectronic applications. E_{fl} and ϕ were calculated using the following equations:

$$E_{fl} = (E_{HOMO}+E_{LUMO})/2 \quad (10)$$
$$\phi = E_{vac}-E_{fl} \quad (11)$$

Here, the vacuum energy level (E_{vac}) is the energy barrier preventing the electron from being completely separated from the material [52].

3. Experimental

HPS and HPG molecules were purchased from Sigma-Aldrich Co. LLC. in solid form with a purity of above 97%. UV-vis absorbance spectra were obtained in chloroform solvent at room temperature using a UV-1800 spectrophotometer (Shimadzu).

4. Results and discussion

4.1. Geometric structures and electronic properties

The monomer structures of HPS and HPG optimized at the DFT/B3LYP/6-311++G(d,p) level of theory are portrayed in Figure 1 (a, b). The total energies of HPS and HPG were calculated to find the most stable structure. The most stable molecule is the one with the lowest energy [53]. The energy of the HPS molecule was –1832.21106368 a.u and the energy of the HPG molecule was –3619.68363740 a.u. This result showed that the HPG molecule was more stable than HPS.

Determining the interaction between a molecule and beam is vital to understand its electronics and to design new photovoltaic devices [54]. The computed absorption wavelengths in chloroform solvent by using TD-DFT/B3LYP/6-311++G(d,p) level theory are listed in Table 1. The computed absorption wavelength of the HPS was at 346 nm (3.59 eV). The major transition was from H→L. The second and third peaks were calculated at 284 (4.36 eV) and 266 nm (4.66 eV) with the transition from H-1→L and H-2→L, respectively. It was determined that the maximum absorbance peaks of HPG had H→L, H-1→L, and H-2→L transitions at wavelengths of 354 nm (3.50 eV), 281 nm (4.41 eV) and 266 nm (4.66 eV), respectively.

The experimental and theoretical absorbance spectra curve of HPS and HPG are shown in Figure 2. Here, it was observed that HPS gave a maximum absorbance peak at 252 nm (4.92 eV) and HPG at 355 nm (3.49 eV), experimentally.

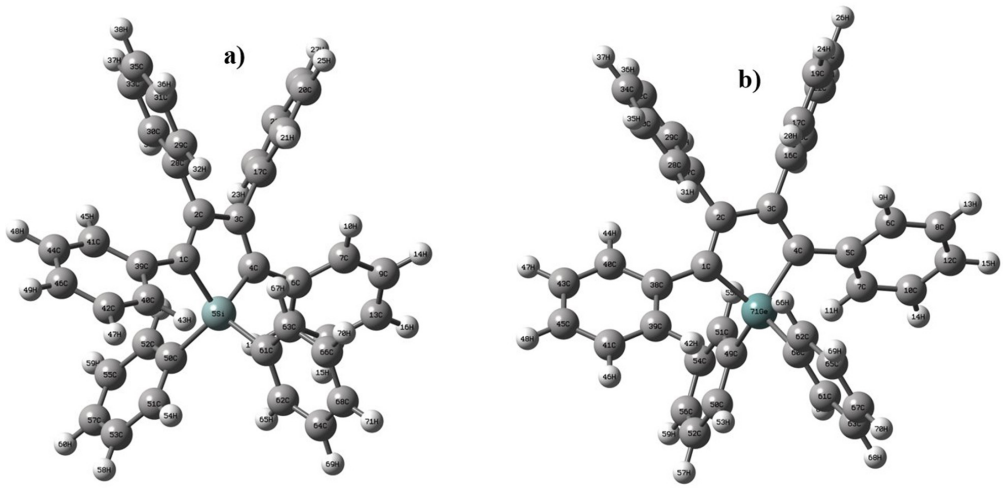

Figure 1. Optimized molecular structures of a) HPS and b) HPG.

Table 1. The computed absorption wavelengths, excitation energies, absorbance, and oscillator strengths.

	λ (nm)	***E (eV)***	***f***	**Transition**
HPG	354	3.50	0.2131	H→L
	281	4.41	0.1318	H–1→L
	266	4.66	0.1522	H–2→L
HPS	346	3.58	0.2483	H→L
	284	4.36	0.0545	H–1→L
	266	4.66	0.2210	H–2→L

Tang and his colleagues [25] observed the experimental maximum absorbance spectrum in chloroform solvent of HPS at about 250 nm. This result is in good agreement with our result. Zhang et al. [22], measured the experimental absorbance spectrum of HPS as approximately 350 nm. The small difference between this result and our measurement could be due to the difference in phases while in our experiment HPS was in chloroform solution, it was in a solid state in the work done by Zhang et al. [22]. Wu et al. [23] also measured the experimental maximum absorbance spectrum of HPS in toluene solvent as approximately 450 nm.

From the theoretical absorbance spectra calculated by the TD-DFT method in Figure 2, it was seen that HPS and HPG molecules had a maximum absorbance spectrum of 270 nm (4.59 eV) and 346 nm (3.58 eV), respectively. Therefore, it can be concluded that they are compatible with both experimental results and literature [25]. In addition, the absorbance spectra of both are in the near ultraviolet region.

Frontier molecular orbitals called HOMO, LUMO and the energy difference between these orbitals are important in terms of charge transfer. Figure 3 (a, b) shows the contour plots of the HOMO and LUMO molecular orbitals and the energy values of these orbitals for the studied molecules. As seen in Figure 3 (a, b), the phenyl rings attached to the silole and germanium atoms in both molecules do not contribute to the HOMO and LUMO orbitals. As seen in Table 2, the energies of the HOMO orbitals were calculated as –7.20 eV for HPG and –6.83 eV for HPS. A molecule with a large HOMO energy level means that it has a more favorable hole transport and thus a hole transfer integral [55]. Therefore, the HOMO of HPS was higher in terms of hole-creating potential. The lower the LUMO energy level of a molecule, the higher its electron injection ability and the more stable the injected electron [56]. The energy LUMO orbital of HPG's (–3.62 eV) was lower than that of HPS (–3.18 eV). Therefore, it indicated a higher electron injection ability of HPG.

The difference between the HOMO and LUMO energy levels, called the electrochemical band gap, and the excitation energy for the transitions between the vertical bands, called the optical band gap, are different energies [57]. The optical band gap is obtained by taking the difference between the vertically excited energy levels from the calculation of the excited energy levels. Here, using the TD-DFT method, electrochemical band gap values of HPG and HPS were calculated as 3.58 eV and 3.65 eV, and optical band gap values were calculated as 3.58 eV and 3.50 eV, respectively (Table 1).

The molecule whose V_{OC} value is closest to the LUMO energy level value is more suitable for efficient photovoltaic devices. For efficient photovoltaic devices, electrons must be able to easily injected from the LUMO into the conduction band of semiconductors [58]. Furthermore, the LUMO of the donor must be higher than the LUMO of the acceptor. As seen in Table 2, the V_{OC} value of HPG was more suitable for photovoltaic device technology and can perform electron transfer with smaller energy (0.852 eV). The work function, which determines the minimum energy required for an electron lifted from the Fermi level to the vacuum level, limits the potential barrier for electron emission.

4.2. Reorganizational energies, ionization potentials and electron affinities

The calculated λ_e/λ_h, IP_a/IP_v, and EA_a/Ea_v values of HPS and HPG molecules are tabulated in Table 3. These calculated values are factors affecting the performance of solar cells. For example, the mobility of electrons and holes is closely related to reorganizational energy. The λ_e value of HPG was calculated to be smaller than that of HPS, and the λ_h value of HPS was calculated to be smaller than that of HGS. Therefore, HPG had potential to be a perfect electron transfer material, and HPS could be excellent hole transfer material.

It is known that the reorganization energy is not sufficient to determine the charge transfer of material. Besides, ionization potentials (IPs), electron affinities (EA's), dipole moments and transfer integral values were calculated and interpreted using computational chemistry methods. Magnitudes such as EA and IP significantly affect the energy threshold available for the injection of holes and electrons in a material. The bigger EA and smaller IP mean better electron and hole transport [59]. In other words, it can be said that n-channel molecules have a higher EA value and p-channel molecules have a smaller IP value [60]. Table 3 shows all $EA_{a/v}$ and $IP_{a/v}$ values of HPS and HPG molecules. The $EA_{a/v}$ and $IP_{a/v}$ values of HPG were 2.231/1.986 eV and 6.639/6.884 eV, respectively. Similarly, the $EA_{a/v}$ and $IP_{a/v}$ values of HPS were 0.816/0.544eV and 4.687/4.959 eV, respectively. Consequently, it can be said that HPG is a good electron transport material and, HPS is the best hole transport material.

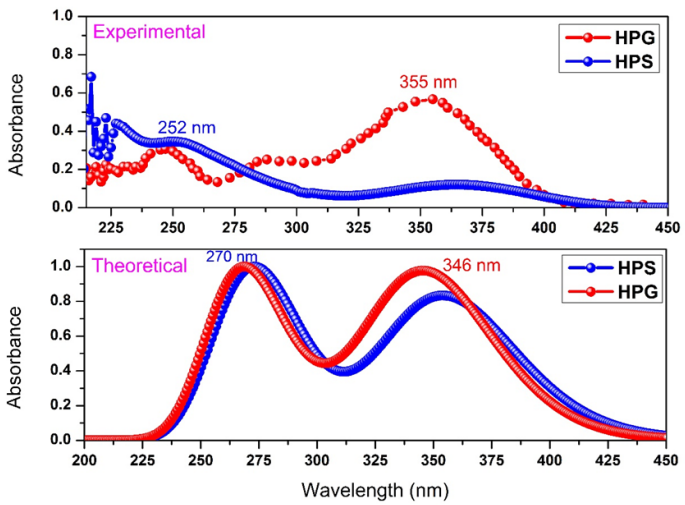

Figure 2. Absorbance spectra curves of HPS and HPG.

Table 2. The HOMO, LUMO, E_{gap}, fermi energy level (E_{fl}), vacuum energy level (E_{vac}) and work function (ϕ). All energies are in eV unit. V_{OC} values are obtained using the LUMO of $PC_{60}BM$ as an acceptor.

Molecules	HOMO	LUMO	E_{gap}	E_{fl}	E_{vac}	ϕ	V_{oc}
HPS	-6.83	-3.18	3.65	-5.005	2.758	2.247	2.936
HPG	-7.20	-3.62	3.58	-5.410	4.558	0.852	3.290

4.3. Dipole moment

Another factor that affects the performance of solar cells is the dipole moment. The dipole moment plays an important role in the production of solar cells as it affects the solubility of a molecule in any solvent [61]. A molecule with a dipole moment is known to have high solubility in chloroform, an organic solvent. For this reason, dipole moments of the studied materials were calculated by using a B3LYP/6-311++G(d, p) basis set in chloroform solvent. As seen in Table 3, HPG had a larger dipole than HPS. Therefore, HPG can self-assemble in the chloroform solvent, indicating that it has greater charge transfer than HPS.

4.4. Effective transfer integrals and charge transfer rates

The effective transfer integrals V represents the strength of the electronic coupling between two neighboring molecules i and j and may vary depending on the geometry of the dimer. Besides, the charge transfer must be anisotropic [39,40,62,63]. Since the interactions between the π-conjugate coupling, which facilitates charge transport between neighboring compounds, are strong, the molecules forming the dimer were considered in parallel while creating the anisotropic geometry. Optimized dimer structures obtained by using parallel dimer geometries for HPG and HPS are given in Figure 4 and transfer integrals belonging to these geometries are tabulated in Table 4. In general, a material with a large transfer integral will also have a large charge transfer. As seen in Table 4, HPG had a higher electron transfer integral (absolute) than HPS. Moreover, the hole transfer integral of HPS was much higher than HPG. Thus, it can be said that HPS is a good candidate for being a hole transfer material.

Charge transfer rates ($W_{electron}$ and W_{hole}) were calculated using equation 1 for HPS and HPG in parallel geometry at room temperature and are tabulated in Table 4. HPG molecule had a high electron transfer rate (530×10^9 s^{-1}). On the other hand, the HPS molecule had a large hole transfer rate (140×10^9 s^{-1}).

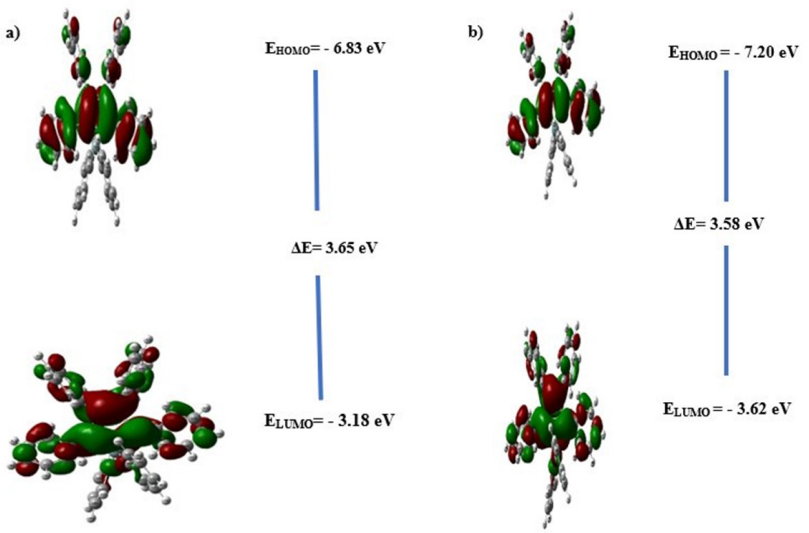

Figure 3. Frontier orbital contour plot a) HPS and b) HPG.

Table 3. The calculated reorganization energies ($\lambda_{electron}$/ λ_{hole}), vertical and adiabatic ionization potentials (IP_a / IP_v), vertical and adiabatic electronic affinities (EA_v/EA_a) (in eV).

Molecules	$\lambda_{electron}$	λ_{hole}	IP_a	IP_v	EA_a	EA_v	Dipole moment (Debye)
HPS	0.417	0.326	4.687	4.959	0.816	0.544	0.0184
HPG	0.244	0.598	6.639	6.884	2.231	1.986	0.1909

Table 4. The charge transfer integrals ($V_{electron}$/ V_{hole}) (in eV) and the charge transfer rates ($W_{electron}$/ W_{hole}) (in s^{-1}).

Molecules	$V_{electron}$	V_{hole}	$W_{electron}$	W_{hole}
HPS	–0.00034	–0.00207	2.6×10^9	140×10^9
HPG	0.00047	0.00002	530×10^9	5×10^9

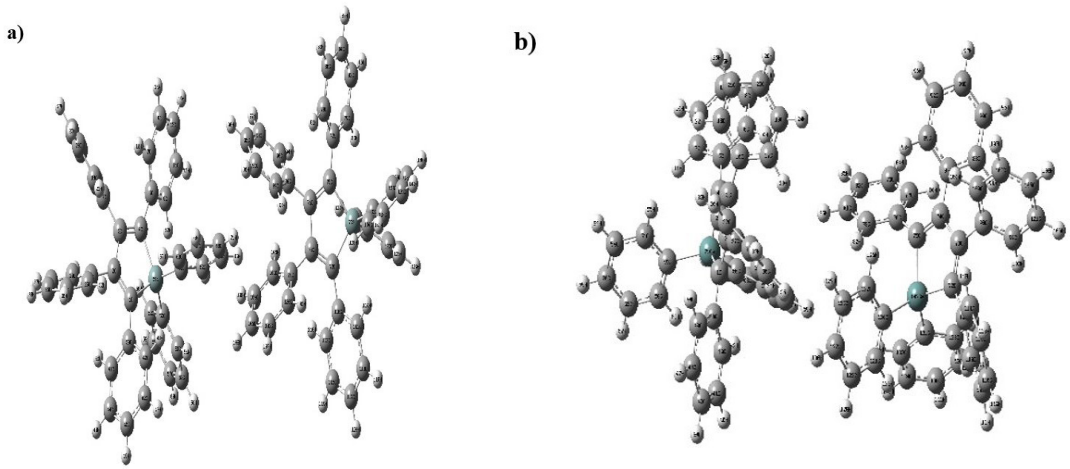

Figure 4. Optimized structure of a) HPS dimer and b) HPG dimer.

4.5. Molecular electrostatic potential (MEP) analysis

The electrostatic molecular potential (MEP) surface, which helps understand the physicochemical structure of a molecule, provides a three-dimensional graphical representation of the molecule depending on its electron density [64]. In this visual presentation, red (negative) regions show electrophilic reactivity which is electron-rich regions, and blue (positive) regions show nucleophilic reactivity which is electron-accepting regions, and green regions show neutral region which is zero potential. MEP studies were carried out using the B3LYP/6-311++G(d,p) basis set and are presented in Figure 5. The color range of the surface was between $–9.131e^{–2}$ and $9.131e^{–2}$, $–8.012e^{–2}$ and $8.012e^{–2}$ for HPS and HPG, respectively. It can be seen from Figure 5 that HPG had more red color intensity showing that HPG is more reactive and electrophilic than HPS.

4.6. NBO analysis

NBO analysis is an efficient method for understanding electron transfer between Lewis (donor (i)) and non-Lewis (acceptor (j)) orbitals [65]. The stabilization energy ($E^{(2)}$), which is a measure of electron transfer by NBO analysis, is estimated by the following equation:

$$E^{(2)} = \Delta E_{ij} = q_i \frac{F(i,j)^2}{\varepsilon_j - \varepsilon_i} \quad (12)$$

where F(i,j), ε_j and ε_i,q_i – were diagonal NBO Fock matrix element, the diagonal elements and the donor orbital occupancy, respectively. NBO analysis was carried out by using NBO 3.1 program [66] included in the Gaussian 09 software. Intramolecular interactions with charge transfer for the most significant stabilization energies E(2), obtained from NBO calculations, are presented in Table 5 and Table 6. The larger the value of E(2), the greater the degree of conjugation or charge transfer of the entire system [67,68]. Compared the calculated NBO results in Table 1 and Table 2 indicated that the stabilization energies of HPG were greater than HPS. For example, the most interesting stabilization energies for HPG were calculated as 21.96 kcal/mol, 19.91 kcal/mol, 25.96 kcal/mol, 41.42 kcal/mol and 74.63 kcal/mol, respectively, which were associated with the donor-acceptor transition of C1-C2→C3-C4, C1-Ge71→C2-C27, C3-C4→C1-C2, C5-C7→C10-C12. On the other side, the most interesting stabilization energies for HPS were calculated as 12.04 kcal/mol, 10.32 kcal/mol, 21.40 kcal/mol, 24.83 kcal/mol, 43.30 kcal/mol, respectively, which are associated with the donor-acceptor transition of C3-C4→C1-C2, C1-Si5→C2-C28, C6-C8→C11-C13, C17-C19→C3-C4, C39-C40→C1-C40. As a result, it was seen that the interaction in HPG is stronger than in HPS.

Table 5. Second order perturbation theory analysis of Fock matrix in NBO basis for HPS.

Donor (i)	Type	ED/e	Acceptor(j)	Type	ED/e	$E^{(2)a}$(KJ mol^{-1})	E(j)-E(i)[b] (a.u)	F(i.j)[c] (a.u)
C1–C2	σ	1.96	C1–Si5	σ*	0.03	2.45	0.99	0.044
C1–C2	π	1.96	Si5–C61	π*	0.03	2.59	0.54	0.034
C1–Si5	σ	1.96	C2–C28	σ*	0.01	10.32	0.94	0.088
C1–C39	σ	1.59	C1–C2	π*	0.31	5.16	1.28	0.073
C1–C39	σ	1.59	C1–Si5	σ*	0.35	4.75	0.91	0.036
C2–C3	σ	1.97	C1–C39	σ*	0.03	4.90	1.11	0.066
C2–C28	σ	1.97	C1–C2	σ	0.03	5.35	1.27	0.074
C2–C28	σ	1.97	C1–Si5	σ*	0.01	2.93	0.90	0.046
C3–C4	π	1.98	C1–C2	π*	0.03	12.04	0.32	0.055
C3–C4	π	1.98	Si5–C61	σ*	0.02	2.32	0.54	0.032
C4–Si5	σ	1.97	C3–C17	σ*	0.03	10.32	0.94	0.088
C6–C8	π	1.97	C11–C13	π*	0.01	21.40	0.28	0.069
C7–C9	π	1.98	C11–C13	π*	0.03	20.50	0.28	0.068
C7–H10	σ	1.98	C6–C8	σ*	0.02	4.41	1.07	0.061
C8–H12	σ	1.98	C6–C7	σ*	0.01	4.35	1.08	0.061
C9–C13	σ	1.97	C7–C9	σ*	0.02	3.19	1.28	0.057
C9-H14	σ	1.97	C6–C7	σ*	0.02	4.31	1.08	0.061
C11–C13	π	1.72	C6–C8	π *	0.5	19.98	0.29	0.068
C17–C19	π	1.72	C22–C24	σ*	0.01	21.08	0.28	0.069
C18–C20	π	1.98	C22–C24	π*	0.03	20.62	0.28	0.068
C28–C29	σ	1.71	C31–C35	σ*	0.31	21.12	0.28	0.069
C30–C33	π*	1.72	C28–C29	σ*	0.47	20.47	0.29	0.069
C39–C40	π	1.72	C1–Si5	π*	0.31	1.06	0.51	0.023
C41–C44	π	1.98	C39–C40	π*	0.02	20.07	0.28	0.068
C50–C51	σ	1.98	Si5–C50	σ*	0.02	2.42	0.97	0.043
C51–C53	σ	1.88	Si5–C50	σ*	0.47	3.20	0.97	0.050
C52–C55	π	1.57	C53–C57	π*	0.47	20.86	0.28	0.069
C53–C57	π	1.57	C50–C51	π*	0.35	22.01	0.28	0.070
C61–C62	σ	1.57	Si5–C61	σ*	0.35	2.42	0.97	0.043
C61–C62	σ		C1–Si5	σ*		0.89	0.52	0.021
C61–C62	π		C63–C66	π*		20.70	0.28	0.069
C61–C63	σ		Si5–C61	σ*		2.52	0.97	0.044
C63–C66	π		C64–C68	π*		20.86	0.28	0.069
C29–C32	π		C27–C28	π*		20.52	0.29	0.069
C6	CR(1)		C4–Si5	σ*		0.76	10.31	0.080
C6–C8	π		C3–C4	π*		63.30	0.01	0.049
C17–C19	π		C3–C4	π*		24.83	0.02	0.036
C39–C40	π		C1–C2	π*		43.30	0.01	0.049
C39–C40	σ		C1–Si5	σ*		1.41	0.01	0.035

Table 6. Second order perturbation theory analysis of Fock matrix in NBO basis for HPG.

Donor (i)	Type	ED/e	Acceptor(j)	Type	ED/e	$E^{(2)a}$(KJ mol^{-1})	E(j)–E(i)[b] (a.u)	F(i.j)[c] (a.u)
C1–C2	σ	1.96	C1–C38	σ*	0.03	4.10	1.22	0.063
C1–C2	σ	1.96	C1–Ge71	σ*	0.03	1.69	0.93	0.036
C1–C2	σ	1.96	C2–C3	σ*	0.01	4.03	1.17	0.061
C1–C2	σ	1.59	C2–C27	σ*	0.31	5.02	1.19	0.069
C1–C2	π	1.59	C3–C4	π*	0.35	21.96	0.32	0.055
C1–C2	π	1.97	C38–C39	π*	0.03	6.33	0.31	0.042
C1–C2	π	1.97	C49–Ge71	π*	0.03	2.12	0.48	0.029
C1–C38	σ	1.97	C1–C2	σ*	0.01	4.91	1.29	0.071
C1–Ge71	σ	1.98	C2–C27	σ*	0.03	19.91	0.94	0.087
C1–Ge71	σ	1.98	C38–C40	σ*	0.02	13.06	1.04	0.053
C2–C3	σ	1.97	C1–C38	σ*	0.03	4.88	1.11	0.059
C2–C3	σ	1.97	C16–C18	σ*	0.01	0.97	0.65	0.024
C2–C27	σ	1.98	C1–C2	σ*	0.03	5.47	1.27	0.075
C2–C27	σ	1.98	C2–C3	σ*	0.02	1.90	1.07	0.040
C3–C4	σ	1.98	C2–C3	σ*	0.01	4.03	1.17	0.061
C3–C4	σ	1.97	C3–C16	σ*	0.02	5.02	1.19	0.069
C3–C4	σ	1.97	C4–Ge71	σ*	0.02	1.69	0.93	0.069
C3–C4	π	1.72	C16–C18	π *	0.5	0.67	0.76	0.022
C3–C4	π	1.72	C1–C2	σ*	0.01	25.96	0.32	0.055
C3–C4	σ	1.98	C5–C7	σ*	0.03	6.33	0.31	0.042
C3–C4	σ	1.71	C60–Ge71	σ*	0.31	2.12	0.48	0.029
C3–C16	σ	1.72	C1–C2	σ*	0.47	1.78	1.27	0.043
C4–C5	σ	1.72	C2–C3	σ*	0.31	3.84	1.29	0.058
C4–C5	σ	1.98	C4–Ge71	σ*	0.02	1.02	0.86	0.027
C4–Ge71	σ	1.98	C1–Ge71	σ*	0.02	11.75	0.68	0.031
C4–Ge71	π	1.88	C3–C16	π*	0.47	19.91	0.94	0.078
C5–C6	π	1.57	C3–C4	π*	0.47	0.85	0.73	0.023
C5–C7	π	1.57	C6–C8	π*	0.35	19.03	0.28	0.066
C5–C7	π	1.57	C10–C12	π*	0.35	41.42	0.28	0.069
C6–C8	π		C5–C7	π*		20.03	0.28	0.068
C10–C12	π		C6–C8	π*		19.93	0.29	0.068
C17–C19	π		C16–C18	π*		40.52	0.29	0.069
C21–C23	π		C16–C18	π*		40.45	0.29	0.069
C29–C32	π		C27–C28	π*		30.52	0.29	0.069
C38–C39	π		C1–Ge71	π*		1.28	0.45	0.023
C49–Ge71	σ		C4–Ge71	σ*		2.56	0.72	0.038
C60–C61	π		C1–Ge71	π*		0.77	0.46	0.018
C60–C61	π		C62–C65	π*		20.61	0.28	0.069
C5–C7	π		C3–C4	π*		74.63	0.02	0.051

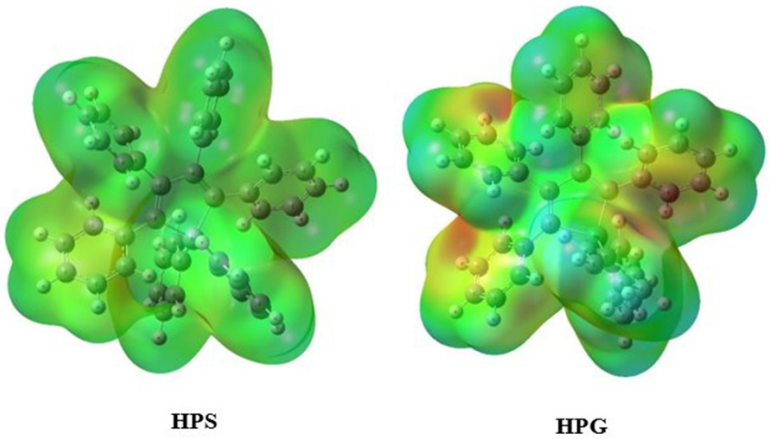

Figure 5. MEP surfaces of the HPS and HPG.

5. Conclusion

In the present study, advanced quantum theoretical calculations were used to examine the charge transfer properties, photovoltaic and electronic properties of HPS and HPG. The absorbance spectra obtained by the experimental analysis method were found to be quite compatible with the calculated absorbance spectra. Structurally, HPG was found to be more stable than HPS due to its lower energy. The reorganization energies and Marcus-Hush theory indicated that HPG can be used as electron transport material and HPS can be used as hole transport material. Through the MEP map, it can be said that HPG was more electrophilic than HPS. These results can also be seen from the values of effective transfer integrals and charge transfer rates. In terms of the calculated work function and open-circuit voltage, it was found that HPG is more suitable for photovoltaic properties. In all the properties obtained, it can be said that the conjugation in the ring was an important factor in the transition from silicon to germanium. Finally, it was determined that HPG was a better candidate than HPS for solar cell devices due to its absorbance spectra, electrochemical, optical band gaps, photovoltaic properties and high E(2) stabilization energy. It is hoped that the results will provide further insight into experimental studies on the design of higher-performance photovoltaic devices.

Declaration of competing interest

The author declares no conflicts of interest.

Acknowledgements

The numerical calculations reported in this paper were performed at TÜBİTAK ULAKBİM, High Performance and Grid Computing Center (TRUBA resources). The author thanks TÜBİTAK ULAKBİM, and the High Performance and Network Computing Center for the numerical calculations used in this article.

References

1. Sabagh S, Izadyar M, Arkan F. Photovoltaic properties of the flavonoid-based photosensitizers: Molecular-scale perspective on the natural dye solar cells. International Journal of Quantum Chemistry 2020; 120 (10): e26171-e26182. doi: 10.1002/qua.26171
2. Manzoor T, Niaz S, Pandith AH. Exploring the effect of different coumarin donors on the optical and photovoltaic properties of azo-bridged push-pull systems: A theoretical approach. International Journal of Quantum Chemistry 2019; 119 (18): e25979-e25994. doi: 10.1002/qua.25979
3. Zhao L, Duan J, Liu L, Wang J, Duan Y et al. Boosting power conversion efficiency by hybrid triboelectric nanogenerator/silicon tandem solar cell toward rain energy harvesting. Nano Energy 2021; 82 (105773): 1-10. doi: 10.1016/j.nanoen.2021.105773
4. Zhang T, An C, Bi P, Lv Q, Qin J et al. A Thiadiazole-based conjugated polymer with ultradeep HOMO level and strong electroluminescence enables 18.6% efficiency in organic solar cell. Advanced Energy Materials 2021; 11 (35): 2101705-2101713. doi: 10.1002/aenm.202101705
5. Duan C, Zhang K, Zhong C, Huang F, Cao Y. Recent advances in water/alcohol-soluble π-conjugated materials: new materials and growing applications in solar cells. Chemical Society Reviews 2013; 42 (23): 9071–9104. doi: 10.1039/C3CS60200A

6. Beaujuge PM, Fréchet JMJ. Molecular design and ordering effects in π-functional materials for transistor and solar cell applications. Journal of American Chemical Society 2011; 133 (50): 20009–20029. doi: 10.1021/ja2073643

7. Facchetti A. π-Conjugated Polymers for Organic Electronics and Photovoltaic Cell Applications. Chemistry of Materials 2011; 23 (3): 733–758. doi: 10.1021/cm102419z

8. Dubac J, Laporterie A, and Manuel G. Group 14 metalloles. 1. Synthesis, organic chemistry, and physicochemical data. Chemical Reviews 1990; 90 (1): 215-263. doi: 10.1021/cr00099a008

9. Tian Z, Yuqian J, Yingli N, Dong W, Qian P et al. Aggregation Effects on the Optical Emission of 1,1,2,3,4,5-Hexaphenylsilole (HPS): A QM/MM Study. Journal of Physical Chemistry A 2014; 118 (39): 9094-9104. doi: 10.1021/jp5021017

10. Saito M, Yoshioka M. The anions and dianions of group 14 metalloles. Coordination Chemistry Reviews 2005; 249 (7): 765-780. doi: 10.1016/j.ccr.2004.08.004

11. Hennig H, Heckner, KH, Pavlov, AA, Kuzmin MG. Spectroscopic properties of silacyclopentadiede derivatives, Reports of the Bunsen Society for Physical Chemistry 1980; 84 (11): 1122-1124. doi: 10.1002/bbpc.19800841108

12. Mullin JL, Tracy JH, Ford JR, Keenan SR, Keenan SR et al. Characteristics of aggregation ınduced emission in 1,1-dimethyl-2,3,4,5-tetraphenyl and 1,1,2,3,4,5-hexaphenyl siloles and germoles. Journal of Inorganic and Organometallic Polymers and Materials 2007; 17 (1): 201-213. doi: 10.1007/s10904-006-9073-4

13. Li JY, Hung CH, Chen CY. Hybrid black silicon solar cells textured with the interplay of copper-induced galvanic displacement. Scientific Reports 2017; 7 (17177): 1-10. doi: 10.1038/s41598-017-17516-6.

14. Dobrzanski LA, Szindler M, Drygała A, Szindler MM. Silicon solar cells with Al_2O_3 antireflection coating. Central European Journal of Physics 2014; 12 (9): 666-670.

15. Allard N, Aich RB, Gendron D, Boudreault PLT, Tessier C et al. Germafluorenes: new heterocycles for plastic electronics. Macromolecules 2010; 43 (5): 2328-2333. doi: 10.1021/ma9025866

16. Miller RD, Wallraff G, Clecak N, Sooriyakumaran R, Michl J et al. Polysilanes: solution photochemistry and deep-UV lithography. Polymer in Microlithography 1989; 412 (25): 115-132. doi: 10.1021/bk-1989-0412.ch008

17. Yabusaki Y, Ohshima N, Kondo H, Kusamoto T, Yamanoi Y et al. Versatile synthesis of blue luminescent siloles and germoles and hydrogen-bond-assisted color alteration. Chemistry A European Journal 2010; 16 (19): 5581-5585. doi: 10.1002/chem.200903408

18. Hwang YM, Ohshita J, Harima Y, Mizumo T, Ooyama Y et al. Synthesis, characterization, and photovoltaic applications of dithienogermole-dithienylbenzothiadiazole and dithienylthiazolothiazole copolymers. Polymer 2011; 52 (18): 3912-3916. doi: 10.1016/j.polymer.2011.07.009

19. Amb CM, Chen S, Graham KR, Subbiah J, Small CE et al. Dithienogermole as a fused electron donor in bulk heterojunction solar cells. Journal of the American Chemical Society 2011; 133 (26): 10062-10065. doi: 10.1021/ja204056m

20. Faustov VI, Egorov MP, Nefedov OM, Molin YN. Ab initio G2 and DFT calculations on electron affinity of cyclopentadiene, silole, germole and their 2,3,4,5-tetraphenyl substituted analogs: structure, stability and EPR parameters of the radical anions. Physical Chemistry Chemical Physics 2000; 2 (19): 4293- 4297. doi: 10.1039/B005247G

21. Zhan X, Risko C, Amy F, Chan C, Zhao W et al. Electron affinities of 1,1-diaryl-2,3,4,5-tetraphenylsiloles: direct measurements and comparison with experimental and theoretical estimates. Journal of American Chemical Society 2005; 127 (25): 9021-9029. doi: 10.1021/ja051139i

22. Zhang T, Jiang Y, Niu Y, Wang D, Peng Q et al. Aggregation effects on the optical emission of 1,1,2,3,4,5-hexaphenylsilole (HPS): A QM/MM study. The Journal of Physical Chemistry A 2014; 118 (39): 9094–9104. doi: 10.1021/jp5021017

23. Wu W, Wang X, Shen M, Li L, Yin Y et al. AIEgens Barcodes Combined with AIEgens Nanobeads for High-sensitivity Multiplexed Detection. Theranostics 2019; 9 (24): 7210-7221. https.//doi.org/10.7150/thno.36525

24. Ito F, Oka N. Use of Aggregation-ınduced emission for selective detection of phase transformation during evaporative crystallization of hexaphenylsilole. Chemistry: An Asian Journal 2019; 14 (16): 755-759. doi: 10.1002/asia.201801563

25. Tang BZ, Zhan X, Yu G, Lee PS, Liu Y et al. Efficient blue emission from siloles. Journal of Materials Chemistry 2001; 11 (12): 2974–2978. doi: 10.1039/B102221K

26. Wang YL, Li QS, Li ZS. End-capped group manipulation of fluorene-based small molecule acceptors for efficient organic solar cells. Computational Materials Science 2019; 156: 252-259. doi: 10.1016/j.commatsci.2018.10.002

27. Zhang L, Shen W, He R, Liu X, Tang X et al. Fine structural tuning of diketopyrrolopyrrole-cored donor materials for small molecule-fullerene organic solar cells: A theoretical study. Organic Electronics 2016; 32 (1): 134-144. doi: 10.1016/j.orgel.2016.01.023

28. Saeed AJMR, Khan MU, Khalid M, Ullah N, Kalgaonkar R et al. Theoretical and conceptual framework to design efficient dye-sensitized solar cells (DSSCs): molecular engineering by DFT method. Journal of Cluster Science 2021; 32 (2): 243–253. doi: 10.1007/s10876-020-01783-x

29. Idrissi S, Labrim H, Bahmad L, Benyoussef A. DFT and TDDFT studies of the new inorganic perovskite CsPbI3 for solar cell applications. Chemical Physics Letters 2021; 766 (7): 138347-138354. doi: 10.1016/j.cplett.2021.138347

30. Nosheen B, Perveen F, Ashraf Z, Bais A, Noor T. Charge transfer and opto-electronic properties of some newly designed polycatenar discotic liquid crystal derivatives: a DFT study. Journal of Molecular Modeling 2020; 26 (291): 1-13. doi: 10.1007/s00894-020-04550-x

31. Üngördü A. Electronic, optical, and charge transfer properties of porphyrin and metallated porphyrins in different media. International Journal of Quantum Chemistry 2019; 120 (6): e26128-e26137. doi: 10.1002/qua.26128

32. Frisch MJ, Trucks, GW, Schlegel HB, Scuseria GE, Robb MA et al. Gaussian 16, Revision C.01, Gaussian, Inc., Wallingford, CT 2016.

33. ADF 2019, SCM, Theoretical Chemistry, Vrije Universiteit, Amsterdam, The Netherlands, http://www.scm.com

34. Wen SH, Li A, Song JL, Deng WQ, Han KL et al. First-principles ınvestigation of anistropic hole mobilities in organic semiconductors. The Journal of Physical Chemistry B 2009; 113 (26): 8813-8819. doi: 10.1021/jp900512s

35. Chai S, Wen SH, Huang JD, Han KL. Density functional theory study on electron and hole transport properties of organic pentacene derivatives with electron-withdrawing substituent. Journal of Computational Chemistry 2011; 32 (15): 3218-3225. doi: 10.1002/jcc.21904

36. Deng WQ, Sun L, Huang JD, Chai S, Wen SH, Han KL. Quantitative prediction of charge mobilities of π-stacked systems by first-principles simulation. Nature Protocols 2015; 10 (2): 632-642. doi: 10.1038/nprot.2015.038

37. Wen SH, Li A, Song JL, Deng WQ, Han KL et al. First-principles ınvestigation of anistropic hole mobilities in organic semiconductors. The Journal of Physical Chemistry B 2009; 113 (26): 8813-8819. doi: 10.1021/jp900512s

38. Chai S, Wen SH, Huang JD, Han KL. Density functional theory study on electron and hole transport properties of organic pentacene derivatives with electron-withdrawing substituent. Journal of Computational Chemistry 2011; 32 (15): 3218-3225. doi: 10.1002/jcc.21904

39. Huang HM, Bellotti P, Chen PP, Houk KN, Glorius F. Allylic C(sp3)-H arylation of olefins via ternary catalysis. Nature Synthesis 2022; 1 (2): 59-68. doi: 10.1038/s44160-021-00006-z

40. Huang JD, Wen SH, Han KL. First-principles ınvestigation of the electronic and conducting properties of oligothienoacenes and their derivatives. Chemistry: An Asian Journal 2012; 7 (5): 1032-1040. doi: 10.1002/asia.201100904

41. Yin S, Yi Y, Li Q, Yu G, Liu Y et al. Balanced carrier transports of electrons and holes in silole-based compounds-a theoretical study. The Journal of Physical Chemistry A 2006; 110 (22): 7138-7143. doi: 10.1021/jp057291o

42. McMahon DP, Troisi A. Evaluation of the External Reorganization Energy of Polyacenes. The Journal of Physical Chemistry Letters 2010; 1 (6): 941-946. doi: 10.1021/jz1001049

43. Sahu H, Panda AN. Computational investigation of charge injection and transport properties of a series of thiophene–pyrrole based oligo-azomethines. Physical Chemistry Chemical Physics 2014; 16 (18): 8563-8574. doi: 10.1039/C3CP55243H

44. Wen Y, Liu Y. Recent Progress in n-Channel Organic Thin-Film Transistors. Advanced Materials 2010; 22 (12): 1331-1345. doi: 10.1002/adma.200901454

45. Wang L, Xu B, Zhang J, Dong Y, Wen S et al. Theoretical investigation of electronic structure and charge transport property of 9,10-distyrylanthracene (DSA) derivatives with high solid-state luminescent efficiency. Physical Chemistry Chemical Physics 2013; 7 (15): 2449-2458. doi: 10.1039/C2CP41876B

46. García G, Moral M, Garzón A. Granadino-Roldán JM, Navarro A et al. Poly(arylenethynyl-thienoacenes) as candidates for organic semiconducting materials. A DFT insight. Organic Electronics 2012; 13 (12): 3244-3253. doi: 10.1016/j.orgel.2012.09.029

47. Li Y, Zou L-Y, Ren A-M, Feng JK. Theoretical study on the electronic structures and photophysical properties of a series of dithienylbenzothiazole derivatives. Computational and Theoretical Chemistry 2012; 981 (1): 14-24. doi: 10.1016/j.comptc.2011.11.021

48. Wolff CM, Caprioglio P, Stolterfoht M, Neher D. Nonradiative recombination in perovskite solar cells: the role of interfaces. Advanced Materials 2019; 31 (52): 1902762-1902769. doi: 10.1002/adma.201902762

49. Scharber MC, Mühlbacher D, Koppe M, Denk P, Waldauf C et al. Design rules for donors in bulk-heterojunction solar cells—towards 10% energy-conversion efficiency. Advanced Materials 2006; 18 (6): 789–794. doi: 10.1002/adma.200501717

50. Alamy AEl, Amine A, Hamidi M, Bouachrine M. Conjugated molecules consisting of thienylenevinylene-co-cyanophenylene as donor materials for bulk heterojunction solar cells. Journal of Materials and Environmental Science 2018; 9 (3): 918-927. doi: 10.26872/jmes.2018.9.3.102

51. Alsufyani W. Spectroscopy of Charge-Transfer States in Non-fullerene Acceptor Organic Solar Cells. Thesis, King Abdullah University of Science and Technology Thuwal, Kingdom of Saudi Arabia, 2019.

52. Kahn A. Fermi level, work function and vacuum level. Material Horiz 2016; 3 (1): 7-10. doi: 10.1039/C5MH00160A

53. Makhov DV, Lewis LJ. Stable Fourfold Configurations for Small Vacancy Clusters in Silicon from ab initio Calculations. Physical Review Letters 2004; 92 (25): 255504. doi: 10.1103/PhysRevLett.92.255504

54. Praveen PL, Ramakrishna DS, Durga PO. UV spectral characterization of a smectic-C liquid crystal: Theoretical support to the experiment. Molecular Crystals Liquids Crystals 2017; 643 (1): 76-82. doi: 10.1080/15421406.2016.1262702

55. Chi WJ, Li ZS. The theoretical investigation on the 4-(4-phenyl-4-α-naphthylbutadieny)-triphenylamine derivatives as hole transporting materials of perovskites-type solar cells. Physical Chemistry Chemical Physics 2015; 17 (8): 5991-5998. doi: 10.1039/C4CP05096G

56. Ahmad I, Abul K, Aijaz RC, Abdullah G.Al-S, Shabbir M, Electro-optical, nonlinear and charge transfer properties of naphthalene based compounds: A dual approach study. Optik 2017; 132 (1): 101–110. doi: 10.1016/j.ijleo.2016.12.023

57. Reynolds JR, Thompson BC, Skotheim TA, Conjugated Polymers Properties, Processing and Applications. (CRC Press, Fourth Edition, Newyork), 61, 2019.

58. Tripathi A, Ganjoo A, Chetti P. Influence of internal acceptor and thiophene based π-spacer in D-A-π-A system on photophysical and charge transport properties for efficient DSSCs: A DFT insight. Solar Energy 2020; 209: 194–205.

59. Rohloff R, Kotadiya NB, Craciun NI, Blom Wetzelaer GAH. Electron and hole transport in the organic small molecule α-NPD. Applied Physics Letters 2017; 110 (7): 073301. doi: 10.1063/1.4976205

60. Hosoi Y, Tsunami D, Ishii H, Furukawa Y. Air-stable n-channel organic field-effect transistors based on N,N′-bis(4-trifluoromethylbenzyl) perylene-3,4,9,10-tetracarboxylic diimide. Chemical Physics Letters 2007; 436 (1): 139–143. doi: 10.1016/j.cplett.2006.12.106

61. Prasad MVS, Sri NU, Veeraiah V. A combined experimental and theoretical studies on FT-IR, FT-Raman and UV–vis spectra of 2-chloro-3-quinolinecarboxaldehyde. Spectrochimica Acta Part A: Molecular Biomolecular Spectroscopy 2015; 148 (5): 163–174. doi: 10.1016/j.saa.2015.03.105

62. Wen SH, Li A, Song JL, Deng WQ, Han KL et al. First-Principles Investigation of Anistropic Hole Mobilities in Organic Semiconductors. Journal of Physical Chemistry B 2009; 113 (26): 8813-8819. doi: 10.1021/jp900512s

63. Chai S, Wen SH, Huang JD, Han KL. Density functional theory study on electron and hole transport properties of organic pentacene derivatives with electron-withdrawing substituent. Journal of Computational Chemistry 2011; 32 (15): 3218-3225. doi: 10.1002/jcc.21904

64. Murray J, Sen K. Molecular electrostatic potentials: concepts and applications, 1 st edition, Elsevier, Amsterdam, 1996.

65. Solğun DG, Yıldıko Ü, Özkartal A, Ağırtaş MS. Photovoltaic performance properties, DFT studies, and synthesis of (E)-3-(diphenxy) acrylic acid substituted phthalocyanine complexes. Chemical Papers 2021; 75: 6285–6295. doi: 10.1007/s11696-021-01786-6

66. Foster JP, Weinhold F. Natural hybrid orbitals. Journal of the American Chemical Society 1980; 102 (24): 7211–7218. doi: 10.1021/ja00544a007

67. 67. Lutoshkin MA, Petrov AI, Malyar YN, Kazachenko AS. Interaction ofRare-Earth Metals and some perfluorinated β-diketones. Inorganic Chemistry 2021; 60 (5): 3291–3304. doi: 10.1021/acs.inorgchem.0c03717

68. Öztürk ST, Aksu P, Turan N, Buldurun K, Tanış E et al. Preparation, spectral characterization, ESR measurements and DFT calculations of Schiff base copper(II) complex, Inorganic and Nano-Metal Chemistry 2021; 51 (11): 1546-1552. doi: 10.1080/24701556.2020.1842768.